IEEE Open Journal of
Power Electronics

Received 2 April 2020; revised 7 May 2020; accepted 10 May 2020. Date of publication 15 May 2020;
date of current version 4 April 2020. The review of this article was arranged by Associate Editor Xiong Du.

*Digital Object Identifier 10.1109/OJPEL.2020.2995105*

# Analysis and Design of Grid-Tied Inverter With LCL Filter

**MICHAEL BIERHOFF [1] (Member, IEEE), RAMY SOLIMAN[1], AND JOSÉ R. ESPINOZA C [2] (Senior Member, IEEE)**

[1]Stralsund University of Applied Sciences, Stralsund 18435, Germany
[2]Universidad de Concepcion, Concepcion 53-C, Chile

CORRESPONDING AUTHOR: MICHAEL BIERHOFF (e-mail: michael.bierhoff@hochschule-stralsund.de)

This work was supported in part by the European Social Fonds within the framework of the Excellence Research Program of the state of Mecklenburg-Vorpommern under Project ESF/14 - BM - A55 - 0017/16 and in part by CONICYT / FONDEQUIP / EQM140148, CONICYT/FONDAP / 15110019, and CONICYT / BASAL / FB0008.

**ABSTRACT** The LCL filter represents the state-of-the-art passive interface type for grid tied power converters as a cost and space reducing alternative to single coil solutions for switching harmonic attenuation. However, a simple PI controller can cause instabilities when applied to control the current of this filter. Thus a general analytically closed approach is presented to determine the safe operating areas for both grid current control mode (GCM) and inverter current control mode (ICM), both with and without additional active damping feedback of the capacitor current. The proposed approach consequently applies the Nyquist criterion in the continuous frequency domain, facilitating the determination of very simple expressions of parameter stability limits. These design guidelines, which partially also confirm previous findings, are for the first time summarized all together as the results of proposed approach to aid corresponding controller design.

**INDEX TERMS** PWM inverter, LCL filter, active damping, stability analysis.

## I. INTRODUCTION

LCL filters are commonly applied for the attenuation of switching harmonic content of the grid current of either single or three phase inverters. A corresponding per phase equivalent circuit is presented in Fig. 1. However, even adding just a proportional controller to realize a closed loop current control can cause instabilities, depending on the sample and carrier frequency, the filter's resonance frequency and the value of the proportional gain of the current controller. Many solutions have been proposed to overcome this problem. This includes so-called active damping (AD). AD has been presented as multiloop [1]–[9] or single loop solution. Multiloop AD can be considered a reduced type of state space controller [10], [11] where the capacitor voltage or current is usually fed back in addition to either grid or inverter current. As a reduced number of sensors is preferable, single loop solutions emerged that apply additional phase lifting measures like lead-lag elements and notch filters [12]–[15] or state observers [16]. The former approaches can all be summarized as attempts to implement an additional differential component to

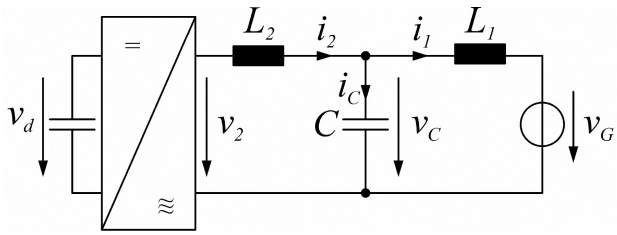


**FIGURE 1.** (Per phase) equivalent circuit of three phase converter with grid side LCL filter.

the single loop controller [17] while at the same time avoiding high frequency perturbation. Previous stability analyses contributed qualitative conclusions from graphical analysis [18] and they were dealing with particular phenomena [19], [20] or certain operation modes such as single loop applications without AD [21]. A full design guideline for the multiloop gain parameter of a GCM with capacitor current feedback is presented in [22]–[24]. However, [22] is a hybrid solution partially referring to a different paper contribution [25]. The

approach presented in [24] determines stability margins of the controller parameters in the continuous frequency domain while accounting for the computational delay time by a graphical solution. Curiously most contributions regarding stability analysis either focus on single or multiloop solutions. Moreover, multiloop stability analysis is usually carried out for GCM only.

The presented contribution can be set apart from existing literature with respect to the following features:

1) *Generality:* A consequently conducted stability analysis approach in continuous frequency domain combined with an a priori current controller design and justified model simplification facilitate the development of simple expressions for either filter or active damping design ensuring stable operation for any kind of control mode (GCM or ICM) or sampling frequency range.
2) *Performance:* The initial PI controller design can also fully be maintained in case of fixed parameter settings (LCL filter, sampling frequency) if proposed dual loop active damping is employed. Thus, no compromise is to be made in terms of system slow pole dynamics.
3) *Implementation:* Thanks to proposed PI controller design unambiguous expressions concerning filter and active damping parameter design were derived adding significant practical relevance to this contribution, see also quick design manual in the appendix. Clearly, no additional parameter tuning is required unless parameter variations are concerned.

Moreover, the proposed analysis results lead to the conclusion that a statically high phase/gain margin does not automatically guarantee immunity against parameter drifts. However, the presented analysis also facilitates an effective modification of the suggested design guide lines to enhance robustness against parameter variation as can easily be seen from a dedicated stability map.

This article is structured as follows. Section II deals with the generic continuous model approach. Essential simplifications are mentioned which make the proposed method applicable not only to single phase but also to three phase applications. In Section III the impact of PWM frequency and method is explained with respect to crucial model parameters. Then the proposed stability analysis is discussed as applied to single current control loops without AD in Section IV. Section V describes the parameter design for dual loop AD as derived from the proposed stability analysis. The proposed analysis approach is also presented in discrete frequency domain for a single design example in Section VI, as comparison to the proposed continuous frequency domain approach. Corresponding measurement results are presented in Section VII, which is followed by a conclusion.

## II. SIMPLIFIED CONTINUOUS MODEL

In three phase applications the LCL filter plant would usually be controlled by a proportional resonant controller in the $\alpha\beta$ reference frame or by a PI controller in the dq reference frame. The fundamental approximation is to neglect

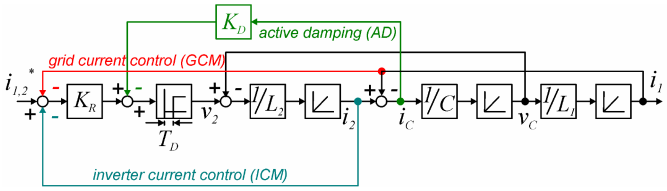


**FIGURE 2.** Simplified block diagram for different current control modes with GCM (red line), ICM (blue line) and AD (green line).

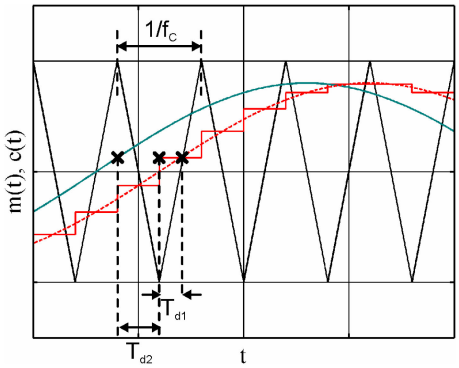


**FIGURE 3.** Retarded discretized modulation waveform (solid red line) with continuous simplification (dashed line) in case of double edge modulation.

the resonant/integral part of the PR/PI controller, which is a reasonable approach [19]–[22] for conventional current controller design. As soon as the controller can be simplified as a pure proportional controller a decoupled representation within the $\alpha\beta$-domain is possible because the controller's transfer function no longer contains any energy storage or state variable that would imply reference domain dependent cross couplings. Furthermore, with the fundamental grid frequency being well below the resonance frequency of the filter, even the cross couplings of the LCL filter model inside the dq-plane can be neglected. The resulting generic simplified continuous model (representing just one current component each, regardless of the reference frame) is shown in Fig. 2, where either the red (GCM) or the blue (ICM) signal path is to be considered as dependent on the current control mode. The green signal traces apply for dual loop active damping, with additional capacitor current feedback.

## III. DEAD TIME COMPOSITION AND CONTROLLER GAIN

### A. ZERO ORDER HOLD APPROXIMATED BY A DEAD TIME

The PWM converter is usually modeled as a sampler with zero order hold element and a corresponding output waveform, as can be seen in Fig. 3. Note, this is an approximation where the corresponding error is discussed in [26] for example. However, the corresponding transfer function $G_{conv}(s)$ of the zero order hold element can be simplified to a dead time $T_{d1}$ facilitating the analysis of high frequency effects. Furthermore, it is common practice to generate the next reference value for the PWM on the basis of a data acquisition that takes place directly after refreshing the PWM registers with the old reference. This retarded data acquisition can be accounted for

by an additional dead time element $T_{d2}$. The resulting transfer function of the converter can be approximated by an overall dead time component summarizing all delays (1).

$$G_{conv}(s) = \frac{1 - e^{-js2T_{d1}}}{s2T_{d1}} e^{-jsT_{d2}} \approx e^{-js(T_{d1}+T_{d2})} = e^{-jsT_D} \tag{1}$$

The determination of $T_D$ is substantially dependent on the acquisition time of the new PWM set value, as can be seen from Fig. 3. From the figure, it is obvious that, regardless of the carrier frequency, a fast acquisition and control algorithm execution can drastically reduce the overall delay time $T_D$. Here the typical outlines for the triangular carrier waveforms and the correspondingly retarded discretized modulation function (red) of a double edge modulation is shown. The blue curve represents an ideal modulation waveform without any time delay. It follows that the overall delay time becomes $T_D = 3/2T_S = 3/(4f_C)$ for the presented double edge modulation with $f_C$ denoting the carrier frequency and $T_S = T_{d2}$ being the sampling time.

### B. PI CONTROLLER DESIGN

The proposed methodology starts with a current controller synthesis to determine the system's slow pole placements. In a second step the overall system stability is investigated, which provides a safe operating area for the system delay time in single loop mode. Based on the given control plant a PI controller is suggested for the dq-reference frame as designed according to the Technical Optimum neglecting the filter capacitor. With the controller transfer function (2) and the filter capacitor being neglected, there follows the design approach (3) and (4) for the PI controller gain and its time constant $T_N$, respectively. With the resistive part of the filter inductors converging to zero, eventually neglecting the integral part obviously seems justified ($T_N \to \infty$).

$$G_R(s) = K_R\left(1 + \frac{1}{T_N s}\right) \tag{2}$$

$$K_R = \frac{L_1 + L_2}{2T_D} \tag{3}$$

$$T_N = \frac{L_1 + L_2}{R_1 + R_2} \tag{4}$$

## IV. STABILITY ANALYSIS FOR SINGLE LOOP CONTROLLERS WITHOUT ACTIVE DAMPING

### A. SAFE OPERATING RANGE FOR THE DELAY TIME

Given the simplified continuous model shown in Fig. 2, the open loop transfer functions for GCM and ICM are given by (5) and (6), respectively. The AD option (green signal lines in Fig. 2) is not activated yet.

$$G_{open,GCM}(j\omega) = \frac{K_R}{j\omega(L_1 + L_2) + (j\omega)^3 L_1 L_2 C} e^{-j\omega T_D} \tag{5}$$

$$G_{open,ICM}(j\omega) = \frac{\left((j\omega)^2 L_1 C + 1\right) K_R}{j\omega(L_1 + L_2) + (j\omega)^3 L_1 L_2 C} e^{-j\omega T_D} \tag{6}$$

The Nyquist criterion can reasonably be applied by creating conditions (7) and (8) with the exponential term turning to imaginary number $j$ if $\omega$ assumes (9) with $n = 0$ for the first real axis crossing of the frequency loci. It can be seen that the numerator as well as the denominator of (7) and (8) will assume real values. The argument of the exponential function that governs the locus orientation is negative, resulting in a clockwise rotational sense. Thus, the frequency response loci for the open loop should cross the real axis in a positive direction (coming from negative to positive imaginary) at values above $-1$ according to Nyquist. Identifying the very first real axis crossing in the positive sense at $n = 0$ the first conditions (10), (11) can be established to determine minimum values for the delay time $T_D$, each. Furthermore, if a controller gain is assumed in accordance with (3), a maximum delay time can be determined as a function of the filter's resonance frequency (12). Proceeding with $n = 1$ in (9) also yields the minimum delay time for GCM. As ICM is inherently stable for low delay times, (13) and (14) already define the safe operating area for the delay time $T_D$ in both cases.

$$\frac{K_R}{j\omega_{crit}(L_1 + L_2) + (j\omega_{crit})^3 L_1 L_2 C} e^{-j\omega_{crit} T_D} \geq -1 \tag{7}$$

$$\frac{\left((j\omega_{crit})^2 L_1 C + 1\right) K_R}{j\omega_{crit}(L_1 + L_2) + (j\omega_{crit})^3 L_1 L_2 C} e^{-j\omega_{crit} T_D} \geq -1 \tag{8}$$

$$\omega_{crit} = (1 + 2n)\frac{\pi}{2T_D} \quad \text{where} \quad n = 0,\ 1,\ 2\ldots \tag{9}$$

$$\frac{K_R}{\left(\frac{\pi}{2T_D}\right)^3 L_1 L_2 C - \frac{\pi}{2T_D}(L_1 + L_2)} \geq -1 \tag{10}$$

$$\frac{\left(1 - \left(\frac{\pi}{2T_D}\right)^2 L_1 C\right) K_R}{\left(\frac{\pi}{2T_D}\right)^3 L_1 L_2 C - \frac{\pi}{2T_D}(L_1 + L_2)} \geq -1 \tag{11}$$

$$\omega_r = \sqrt{\frac{L_1 + L_2}{L_1 L_2 C}} \tag{12}$$

$$\frac{\pi}{2}\sqrt{\frac{\pi}{\pi - 1}}\frac{1}{\omega_r} \leq T_{D,GCM} \leq \frac{3\pi}{2}\sqrt{\frac{3\pi}{1 + 3\pi}}\frac{1}{\omega_r} \tag{13}$$

$$T_{D,ICM} \leq \frac{\pi}{2}\sqrt{\frac{1}{\pi - 1}\left(\pi - \frac{L_1 + L_2}{L_2}\right)}\frac{1}{\omega_r} \tag{14}$$

In Figs. 4 and 5 the frequency response loci of the open loop transfer function of a typical system with filter parameters corresponding to the lab set-up (see Table I) are presented both for GCM in Fig. 4 and ICM in Fig. 5, each for the case of boundary stability operation and a proportional controller with its gain determined according to (3). Note that the dashed lines indicate the infinite arch at singularity case $\omega = \omega_r$, where the loci experience a 180° phase reversal with its clockwise orientation still being determined by the exponential functions of (5) and (6). From these images it becomes obvious that as soon as the delay time exceeds the stability

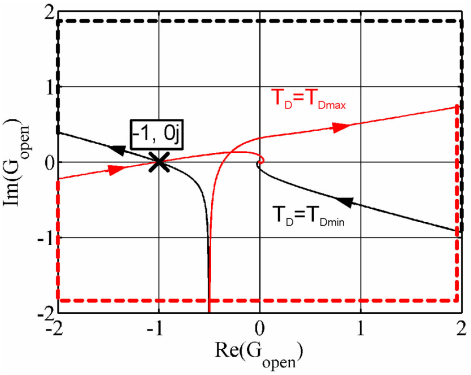


**FIGURE 4.** Frequency response locus for GCM at stability boundary $T_D = T_{Dmin}$ (black) and $T_D = T_{Dmax}$ (red).

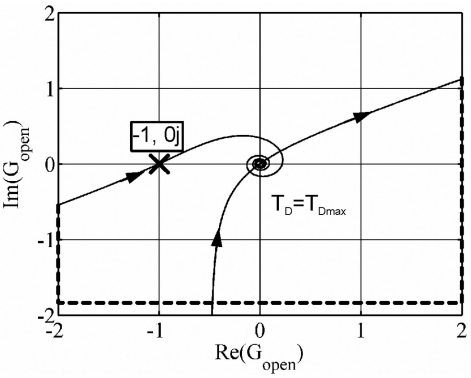


**FIGURE 5.** Frequency response locus for ICM at stability boundary $T_D = T_{Dmax}$.

**TABLE I.** System Parameters

| | |
|---|---|
| DC bus voltage, $V_d$ | 250 V |
| filter inductor 1, $L_1$ | 1.5 mH |
| filter inductor 2, $L_2$ | 1,5 mH |
| filter capacitor, $C$ | 21 µF |
| transformer output voltage (crest value), $V_G$ | 100 V |
| grid frequency, $f_G$ | 50 Hz |
| acquisition mode | double edge |

range the critical point will be encircled and instability is inevitable.

## V. STABILITY ANALYSIS FOR DUAL LOOP CONTROLLERS WITH ACTIVE DAMPING

### A. GCM WITH CAPACITOR CURRENT FEEDBACK AD

The presented analysis method can conveniently be applied to facilitate the design of AD with proportional feedback if the PI controller's integral part is neglected again. For the GCM with capacitor current AD the open loop transfer function is given by (15) where $K_D$ is the additional capacitor current feedback gain, which is still to be determined in terms of safe operating range. One fundamental limit value for $K_D$ could be determined applying the Routh-Hurwitz criterion if the dead time element was approximated by a first order delay [24], [25]. However, following a completely consistent analytical approach maintaining the same model, throughout this presentation the Nyquist criterion will consequently also be applied to solve this problem. In this case, the system frequency is to be assigned the filter's resonance frequency $\omega = \omega_r$ to set up the first stability condition (16). Because with resonance singularity the frequency response locus undertakes a sudden 180° phase shift, it would always cross the real axis unless residing directly on the real axis itself. The corresponding transition from negative to real imaginary must take place above the real part of the Nyquist point (−1). Developing the sufficient condition (16) with (12) a very simple expression (17) is derived that agrees well with previous publications [24], [25]. The limit value (17) represents a special result because it apparently is generally valid regardless of the actual delay time value.

$$G_{open,CC}(j\omega) = \frac{(j\omega)^2 L_1 C K_D + K_R}{j\omega(L_1 + L_2) + (j\omega)^3 L_1 L_2 C} e^{-j\omega T_D} \quad (15)$$

$$\mathrm{Re}\left\{ \frac{(j\omega_r)^2 L_1 C K_D + K_R}{j\omega_r(L_1 + L_2) + (j\omega_r)^3 L_1 L_2 C} e^{-j\omega_r T_D} \right\} \geq -1 \quad (16)$$

$$K_{D,\lim 1} = K_R \frac{L_2}{L_1 + L_2} \quad (17)$$

Now $K_D$ varies between (17) and a second limit. Again referring to (9) with $n = 0$ applied to (15) via condition (18) a second limit value can be found for the damping coefficient $K_D$ (19); this represents a maximum value for $K_D$ for low delay time values. If (3) was applied to substitute $K_R$ then along with (17) being set equal to (19) a time delay limit with respect to the filter's resonance frequency can be determined (20). This delay time represents an operation point were both limit expressions (17) and (19) would converge. For delay time values above that point the corresponding limit values are changing senses, that is the top becomes the bottom limit and vice versa. This operation range will be referred to as 'mode 2' from now on. Examination of the frequency response loci shows that, from a certain delay time on, the second real axis crossing in positive sense also has to be accounted for by using (9) with $n = 1$ in condition (18). A third limit value results for $K_D$ (21) which is the prevailing minimum if 'mode 3' is reached by delay time $T_D$ exceeding expression (22) as current controller gain design (3) was applied.

$$\frac{(j\omega_{crit})^2 L_1 C K_D + K_R}{j\omega_{crit}(L_1 + L_2) + (j\omega_{crit})^3 L_1 L_2 C} e^{-j\omega_{crit} T_D} \geq -1 \quad (18)$$

$$K_{D,\lim 2} = L_2 \left( \frac{\pi}{2T_D} - \frac{2T_D {\omega_r}^2}{\pi} \right) + \frac{K_R}{L_1 C} \left( \frac{2T_D}{\pi} \right)^2 \quad (19)$$

$$T_{D,\lim 1} = \frac{\pi}{2\omega_r} \quad (20)$$

$$K_{D,\lim 3} = L_2 \left( \frac{2T_D {\omega_r}^2}{3\pi} - \frac{3\pi}{2T_D} \right) + \frac{K_R}{L_1 C} \left( \frac{2T_D}{3\pi} \right)^2 \quad (21)$$

$$T_{D,\lim 2} = \frac{3}{2\omega_r} \sqrt{\frac{\pi^3}{3\pi - 2}} \quad (22)$$

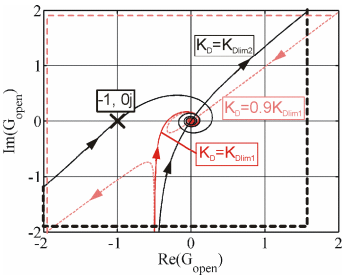


**FIGURE 6.** Frequency response loci (GCM with AD, $T_D = \pi/(4\omega_r)$ (mode 1) with capacitor current feedback, $K_D = K_{Dlim1}$ (red) and $K_D = K_{Dlim2}$ (black).

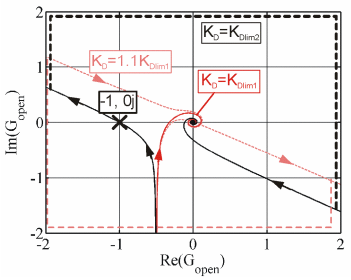


**FIGURE 7.** Frequency response loci (GCM with AD, $T_D = 2\pi/(3\omega_r)$ (mode 2) with capacitor current feedback, $K_D = K_{Dlim1}$ (red), and $K_D = K_{Dlim2}$ (black).

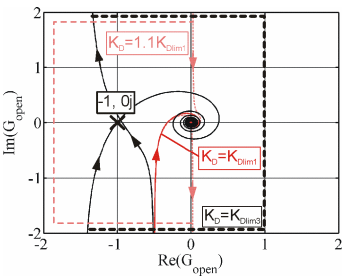


**FIGURE 8.** Frequency response loci (GCM with AD, $T_D = \pi/\omega_r$ (mode 3) with capacitor current feedback, $K_D = K_{Dlim1}$ (red), and $K_D = K_{Dlim3}$ (black).

Different frequency response loci of the open loop transfer function of actively damped GCM with capacitor current feedback are presented in Figs. 6–8. The parameters are still the same as for the laboratory set-up but now different delay times are assumed representing an ideal operation point of modes 1–3 each. The red curve always indicates the frequency response locus with $K_D = K_{Dlim1}$ while the black always shows the locus for the second valid limit value of $K_D$. If the value of $K_D$ exceeds the stable operation range at limit value $K_{Dlim1}$ the open loop frequency response locus drastically changes appearance to an obviously unstable outline. Depending on the respective operation mode, this can be either a positive or a negative limit value excess. In order to demonstrate this behavior the frequency response loci for a 10% deviation with respect to $K_{Dlim1}$ are also included (light red) representing an unstable example each.

### B. ICM WITH CAPACITOR CURRENT FEEDBACK AD

The inverter current control mode can be extended to lower frequencies with respect to the single loop control version by introducing additional proportional feedback AD. Feeding back the capacitor current does not have any effect in the high carrier frequency range but it helps to extend the operating range to lower carrier frequencies than for the single loop solution. The corresponding open loop transfer function would be given by (23) for ICM. For stability a generally valid limit value for proportional gain $K_D$ can be determined in the same fashion as before by stability condition (17) with a negative result in this case (24). Once again applying (9) with $n = 0$ to (23) the resulting stability condition (25) can be developed to determine the top limit of the stability range of $K_D$, see (26). With (3) being substituted in (26) which in turn is set equal to (24) a time delay limit is found that coincides with the previously found value for GCM (20). From this time delay limit value, the stability limits for $K_D$ are again switching senses as (24) is now describing the maximum and (26) yields the minimum for $K_D$ (transition from operation mode 1 to mode 2). But the minimum has to be carefully examined as a second turn around of the locus could still compromise stability. The same time delay limit that was determined before, (22), also indicates the transition from operation mode 2 to 3 for ICM where the corresponding third stability condition governs the actual bottom limit for $K_D$ (27). The open loop frequency response loci of the ICM with capacitor current feedback AD are actually looking the same as the ones for GCM in Figs. 6–8, which is why no corresponding images are shown here.

$$G_{open,CC}(j\omega) = \frac{(j\omega)^2 L_1 C (K_R + K_D) + K_R}{j\omega (L_1 + L_2) + (j\omega)^3 L_1 L_2 C} e^{-j\omega T_D} \quad (23)$$

$$K_{D,\lim 1} = -K_R \frac{L_1}{L_1 + L_2} \quad (24)$$

$$\frac{(j\omega_{crit})^2 L_1 C (K_R + K_D) + K_R}{j\omega_{crit} (L_1 + L_2) + (j\omega_{crit})^3 L_1 L_2 C} e^{-j\omega_{crit} T_D} \geq -1 \quad (25)$$

$$K_{D,\lim 2} = \frac{\pi L_2}{2T_D} - \frac{2T_D L_2 {\omega_r}^2}{\pi} + \left( \frac{1}{L_1 C} \left( \frac{2T_D}{\pi} \right)^2 - 1 \right) K_R \quad (26)$$

$$K_{D,\lim 3} = \frac{2T_D L_2 {\omega_r}^2}{3\pi} - \frac{3\pi L_2}{2T_D} + \left( \frac{1}{L_1 C} \left( \frac{2T_D}{3\pi} \right)^2 - 1 \right) K_R \quad (27)$$

### C. SIMILARITIES BETWEEN GCM AND ICM WITH AD

For the application of the proposed active damping a uniform transfer function of the open current control loop results (28), if the active damping coefficient was designed according to (17) for GCM and (24) for ICM. With these AD settings the resulting zeros are obviously completely compensating for the high frequency conjugate complex pole pair. Furthermore, transfer function (28) delivers best reference step responses with the dedicated PI controller being designed according to the Technical Optimum which confirms initial approach (3). Since the suggested controller gain yields a unique frequency

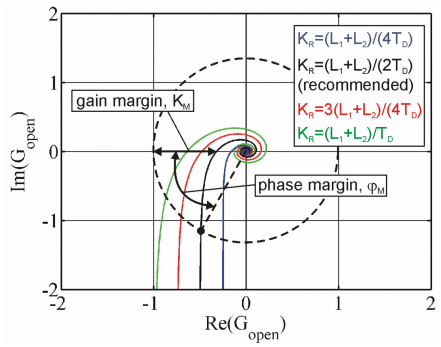


**FIGURE 9.** **Uniform frequency response loci (GCM and ICM with capacitor current feedback AD, $K_D = K_{Dlim1}$) with different controller gains.**

response locus, regardless of the delay time, it follows a uniform expression for the phase and gain margins (29), (30), see also Fig. 9.

$$G_{open,CC}(j\omega) = \frac{K_R e^{-j\omega T_D}}{j\omega\,(L_1 + L_2)} \tag{28}$$

$$\phi_M = \frac{\pi}{2} - \frac{K_R T_D}{L_1 + L_2} \tag{29}$$

$$K_M = 1 - \frac{K_R T_D}{\pi\,(L_1 + L_2)} \tag{30}$$

## VI. COMPARISON WITH DISCRETE FREQUENCY DOMAIN APPROACH

The presented approach of using the Nyquist criterion for stability analysis can also be carried out in the discrete frequency domain as proposed in [21]. But since the derivation of correspondences to (13) and (14) would yield transcendental equations for the sampling time $T_S$ only the determination of discrete system correspondences for equations (17) and (19), which are the limit values of $K_D$ for GCM with capacitor current feedback AD, are presented. The corresponding open loop transfer function can be given by (31).

$$G_{open,CC}(z) = \frac{1}{(L_1 + L_2)\,z} \left(\frac{K_R T_S}{z-1} + \frac{\sin(\omega_r T_S)\,(z-1)}{z^2 - 2z\cos(\omega_r T_S) + 1}\left(\omega_r K_D L_1 C - \frac{K_R}{\omega_r}\right)\right) \tag{31}$$

Note that the sampling time $T_S$ is equivalent to delay time $T_{d2}$ in (1). Condition (32) can be set up in correspondence to (16) for the case of $z = e^{j\omega T_S}$ with $\omega = \omega_r$. The overall denominator of expression (31) comes to zero for this case, which is again drastically simplifying the problem down to expression (33), again coinciding with (17). This is an important finding as it proves again the general validity of this unique limit value.

$$\mathrm{Re}\left(G_{open,CC}\left(z = e^{j\omega_r T_S}\right)\right) \geq -1 \tag{32}$$

$$\omega_r K_D L_1 C - \frac{K_R}{\omega_r} \geq 0 \Leftrightarrow K_D \geq \frac{K_R}{L_1 C {\omega_r}^2} \tag{33}$$

The correspondence of the second limit value can be found by substituting $\omega = \pi/(3T_S)$ into $z = e^{j\omega T_S}$ for expression (31) because this characteristic value would yield the first positive zero crossing of the imaginary part of the open loop frequency response locus. According to Nyquist the remaining real part should reside above the characteristic point of $-1$ which is expressed by condition (34). Solving (34) for $K_D$ yields (35) as a discrete correspondence to (19). With the parameter settings of Table I and (3) being applied at a carrier frequency of 5 kHz the continuous approach would yield $K_{Dlim2,con} = 10.96$ V/A while the discrete method results in $K_{Dlim2,dis} = 10.83$ V/A.

$$G_{open,CC}\left(z = e^{j\frac{\pi}{3}}\right) = \frac{1}{L_1 + L_2} \left(\frac{\sin(\omega_r T_S)}{1 - 2\cos(\omega_r T_S)}\left(\omega_r K_D L_1 C - \frac{K_R}{\omega_r}\right) - K_R T_S\right) \geq -1 \tag{34}$$

$$K_{D\lim 2} = \frac{L_2}{L_1 + L_2}\left(\frac{(K_R T_S - L_1 - L_2)\,\omega_r\,(1 - 2\cos(\omega_r T_S))}{\sin(\omega_r T_S)} + K_R\right) \tag{35}$$

From this section it can be concluded that continuous and discrete approach can both be applied to determine certain stability figures. However, there are typical benefits and drawbacks for either method. The discrete approach offers the opportunity to also account for the stability impact of the integral part of the PI controller as presented in [21] which is only numerically possible for the continuous approach. But since the integral part effect of the PI controller can be neglected with the proposed design approach another important property of the continuous frequency domain model counts: Analytical determination of delay time limits is only possible with the continuous frequency domain model. This applies especially to single loop stability limits (13) and (14) as well as for important operation mode boundary (20).

## VII. EXPERIMENTAL RESULTS

### A. STABILITY MAP

The experiment was carried out with a PI controller designed according to (2) – (4). Limit values of the damping coefficients $K_D$ of capacitor current feedback AD for GCM (black) and ICM (red) are given in the stability map of Fig. 10 versus normalized delay time as they apply for the actual test rig. The adjacent black and red graphs (hatched areas) are representing safe operation ranges for $K_D$, each. Consequently, the zero crossings of $K_{Dlim2}$ and $K_{Dlim3}$ (not visible in this diagram) delimit the single loop stability ranges. In fig. 10 the location of each measurement point is given inside the stability map, also compare with Fig. 13. Transition between these operation points was only realized by varying the carrier frequency and the AD feedback coefficient $K_D$. Neither passive LCL filter nor the sampling mode was otherwise altered during the entire experiment. However, as the carrier frequency varies the

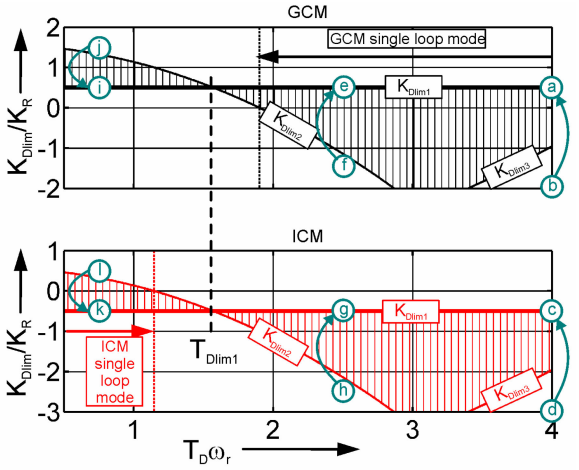


**FIGURE 10.** Stability map: AD gain limits (capacitor current feedback) versus normalized delay time for GCM (black) and ICM (red).

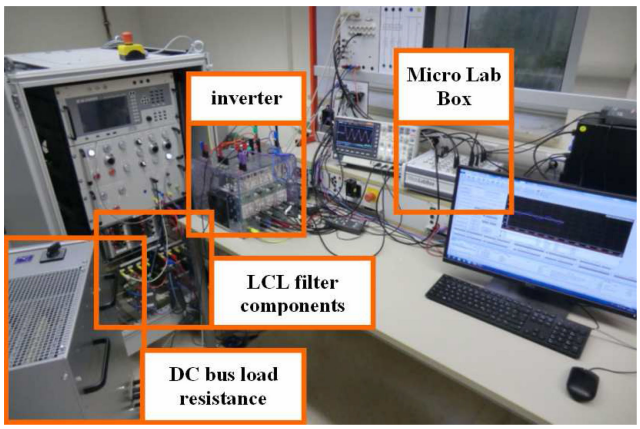


**FIGURE 11.** Laboratory test set-up.

proportional gain of the PI controller is dynamically adjusted according to (3), of course.

### B. MEASUREMENT RESULTS

A two-level three phase IGBT converter was coupled to the grid via an LCL filter and a succeeding transformer with a reduced voltage, see also Figs. 11 and 12. The primary side stray inductance is to be divided by the square of the voltage ratio to determine its secondary side equivalent .It results a total stray inductance (with respect to the secondary side) of approximately 100µH. This value is actually to be added to filter inductance $L_1$ but was neglected for the theoretical analysis. The PLL bandwidth was well chosen below the fundamental grid frequency to avoid any PLL instability interference, see also [27] for further details. The capacitor current was reconstructed by the difference of inverter and line current. The PWM was operated in double edge sampling mode, as shown in Fig. 3. All relevant parameter details can be found in Table I.

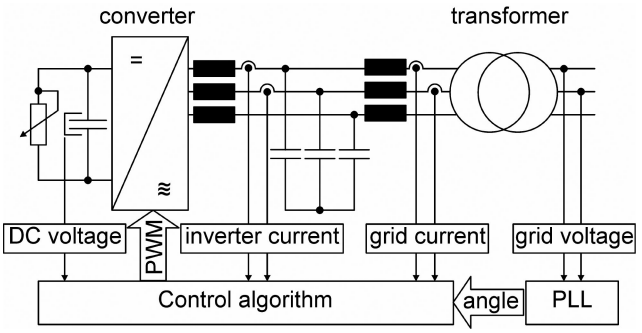


**FIGURE 12.** Equivalent circuit of laboratory test set-up.

Reference step responses were measured for one exemplary grid (blue) and inverter (red) phase current, respectively. The current controller (dq reference frame) was provided with reference steps of either $i_{1q}* = 10$ A (GCM) or $i_{2q}* = 10$ A (ICM) depending on the control mode. Furthermore, the AD feedback gain $K_D$ was suddenly assigned values deviating from the proposed optimum to demonstrate the resulting suboptimal operation. The instantaneous value of $K_D/K_R$ is presented by a black trajectory for all cases where such transition was recorded.

Basically three different carrier and thus sampling frequencies were tested. As a reference for each operating point a current reference step response was recorded where the proposed optimal feedback coefficient $K_{Dlim1}$ was applied in a dual loop AD according to (17) for GCM and (24) for ICM. As already explained in section V-C these damping coefficient values provide maximum gain margins to the system. However, at the same time they are representing safe operating area boundaries as can also be seen from Fig. 10. Thus, a second measurement was conducted for each of these sampling frequencies and control modes (GCM and ICM) starting with $K_D$ to assume values of the opposite stability boundary and even beyond with a sudden step back to optimal values of $K_D = K_{Dlim1}$. The measurement results support the claim that maximal phase and gain margins can be expected as the value of $K_D$ converges against the thick lines of the stability map (oscillations are reduced). Secondly, they also indicate that the stability map seems to represent a worst case scenario as it neglects natural damping effects. All different operation points for the measurement results presented in Fig. 13 are also listed by Table II.

For operating points leaving the stable operating area at the thick line edge (exceeding stable operating area at $K_{Dlim1}$) a stability margin of up to $\pm 0.5\ K_{Dlim1}/K_R$ was observed. However, stability is rapidly lost beyond that limit and operation is usually interrupted by overcurrent faults. Hence, in order to preserve robustness against parameter variations it is recommended to move the AD feedback coefficient value further into the safe operating area that is $K_D > K_{Dlim1}$ for $T_D < T_{Dlim1}$ and $K_D < K_{Dlim1}$ for $T_D > T_{Dlim1}$ where $T_{Dlim1} = \pi/(2\omega_r)$, see also (20).

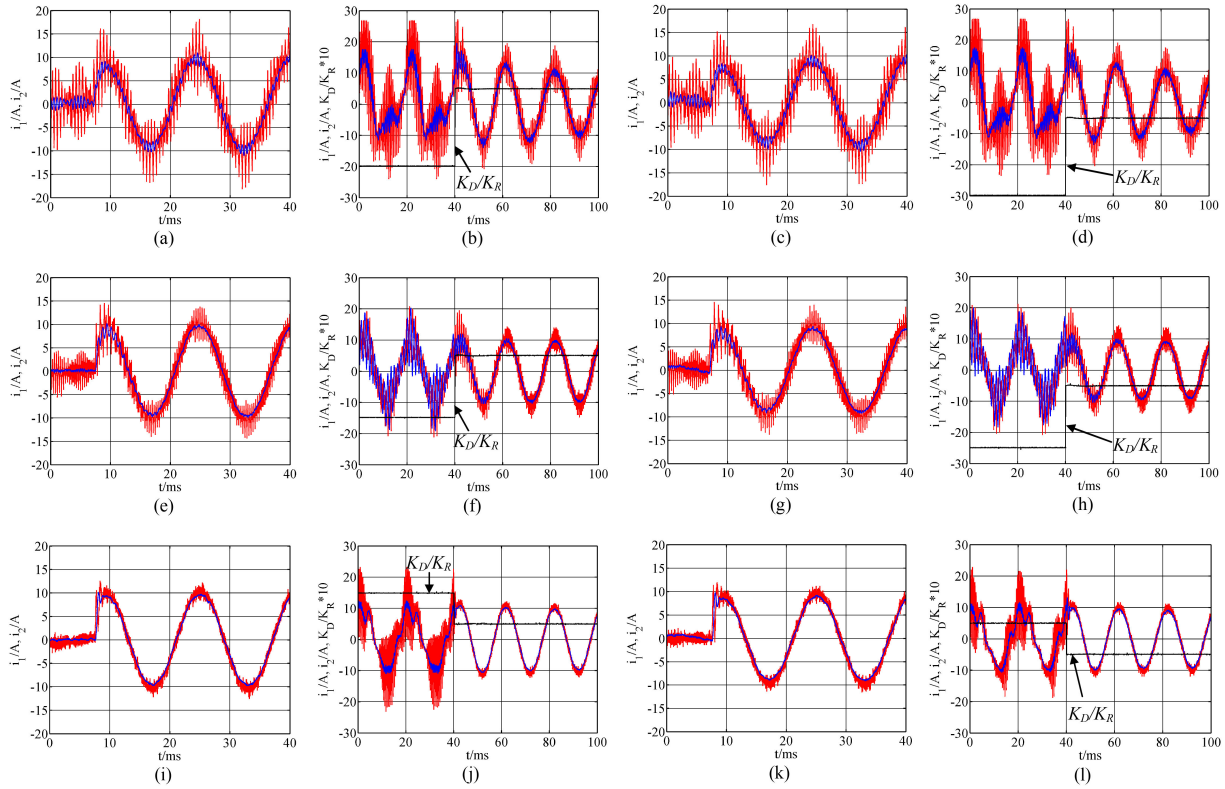


**FIGURE 13.** Measurement results for phase current values of $i_1$ (blue) and $i_2$ (red) in case of $f_C = 1.5$ kHz (GCM: a, b, ICM: c, d), $f_C = 2.4$ kHz (GCM: e, f, ICM: g, h) and $f_C = 8$ kHz (GCM: i, j, ICM: k, l); in case of varying $K_D$ the black trajectory represents parameter $K_D/K_R$.

**TABLE II.** Measurement points (MP)

| MP | mode | $f_C$/kHz | $T_D\omega_r$ | $i_{1q}^*$/A | $i_{2q}^*$/A | $K_D/K_R$ |
|---|---|---|---|---|---|---|
| a) | GCM | 1.5 | 4 | 0→10 | - | 0.5 |
| b) | GCM | 1.5 | 4 | 10 | - | -2 → 0.5 |
| c) | ICM | 1.5 | 4 | - | 0→10 | -0.5 |
| d) | ICM | 1.5 | 4 | - | 10 | -3 → -0.5 |
| e) | GCM | 2.4 | 2.5 | 0→10 | - | 0.5 |
| f) | GCM | 2.4 | 2.5 | 10 | - | -1.5 → 0.5. |
| g) | ICM | 2.4 | 2.5 | - | 0→10 | -0.5 |
| h) | ICM | 2.4 | 2.5 | - | 10 | -2.5 → -0.5 |
| i) | GCM | 8.0 | 0.75 | 0→10 | - | 0.5 |
| j) | GCM | 8.0 | 0.75 | 10 | - | 1,5 → 0.5 |
| k) | ICM | 8.0 | 0.75 | - | 0→10 | -0.5 |
| l) | ICM | 8.0 | 0.75 | - | 10 | 0.5 → -0.5 |

**TABLE III.** Parameter Design Overview

| | | |
|---|---|---|
| 1) | Recommended proportional gain for PI controller, $K_R$ | $\frac{L_1+L_2}{2T_D}$ |
| 2) | Recommended integral time constant for PI controller, $T_N$ | $T_N = \frac{L_1+L_2}{R_1+R_2}$ |
| 3) | Minimum delay time GCM without AD, $T_{Dmin}$ | $\frac{\pi}{2}\sqrt{\frac{\pi}{\pi-1}}\frac{1}{\omega_r}$ |
| 4) | Maximum delay time GCM without AD, $T_{Dmax}$ | $\frac{3\pi}{2}\sqrt{\frac{3\pi}{1+3\pi}}\frac{1}{\omega_r}$ |
| 5) | Maximum delay time ICM without AD, $T_{Dmax}$ | $\frac{\pi}{2}\sqrt{\frac{1}{\pi-1}\left(\pi-\frac{L_1+L_2}{L_2}\right)}\frac{1}{\omega_r}$ |
| 6) | Recommended AD feedback gain (capacitor current) for GCM, $K_D$ | $\frac{L_2}{2T_D}$ |
| 7) | Recommended AD feedback gain (capacitor current) for ICM, $K_D$ | $-\frac{L_1}{2T_D}$ |

## VIII. CONCLUSION

The presented stability analysis offers the opportunity to design a robust single loop current controller as applied to LCL filters. Combined with proposed PI controller design for fast dynamic response it also helps to overcome corresponding single loop stability restrictions by associated dual loop AD design procedure. Hence, the simple overall design guide line provided by Table III (appendix) supports the current controller design as it maintains constant phase margin at consistent dynamical performance versus the entire carrier frequency range for both GCM and ICM.

Moreover, the analysis results clearly suggest that AD coefficient limit values (17) and (24) not only yield maximum gain margins but also represent stability boundary values that are not necessarily only minima as commonly assumed. Experimental results confirm the theoretically derived safe operating area as a global orientation in terms of stability. The fact that parasitic natural damping is neglected in the original analysis yields a worst case scenario with some stability margin.

## APPENDIX

Table III is summarizing the most important results of proposed analysis for a swift implementation. Apply 1) and 2) for

PI controller design, then check stability for single loop mode either with 3) and 4) for GCM or with 5) for ICM. In case of no stability confirmed either modify LCL filter or apply AD with 6) for GCM or 7) for ICM.

## REFERENCES

[1] E. Twining and D. G. Holmes, "Grid current regulation of a three-phase voltage source inverter with an LCL input filter," *IEEE Trans. Power Electron.*, vol. 18, no. 3, pp. 888–895, May 2003.

[2] V. Blasko and V. Kaura, "A novel control to actively damp resonance in input LC filter of a three-phase voltage source converter," *IEEE Trans. Ind. Appl.*, vol. 33, no. 2, pp. 542–550, Mar./Apr. 1997.

[3] P. C. Loh and D. G. Holmes, "Analysis of multiloop control strategies for LC/CL/LCL-filtered voltage-source and current-source inverters," *IEEE Trans. Ind. Appl.*, vol. 41, no. 2, pp. 644–654, Mar./Apr. 2005

[4] E. Wu and P. W. Lehn, "Digital current control of a voltage source converter with active damping of LCL resonance," *IEEE Trans. Power Electron.*, vol. 21, no. 5, pp. 1364–1373, Sep. 2006.

[5] M. Malinowski and S. Bernet, "A simple voltage sensorless active damping scheme for three-phase PWM converters with an LCL filter," *IEEE Trans. Ind. Electron.*, vol. 55, no. 4, pp. 1876–1880, April 2008

[6] M. H. Bierhoff and F. W. Fuchs, "Active damping for three-phase PWM rectifiers with high-order line-side filters," *IEEE Trans. Ind. Electron.*, vol. 56, no. 2, pp. 371–379, Feb. 2009

[7] J F. Liu, Y. Zhou, S. Duan, J. Yin, B. Liu, and F. Liu, "Parameter design of a two-current-loop controller used in a grid-connected inverter system with LCL filter," *IEEE Trans. Ind. Electron.*, vol. 56, no. 11, pp. 4483–4491, Nov. 2009

[8] J. Dannehl, F. W. Fuchs, S. Hansen, and P. Thogersen, "Investigation of active damping approaches for PI-based current control of grid-connected pulse width modulation converters with LCL filters," *IEEE Trans. Ind. Appl.*, vol. 46, no. 4, pp. 1509–1517, Jul./Aug. 2010.

[9] Y. Tang, P. C. Loh, P. Wang, F. H. Choo, F. Gao, and F. Blaabjerg, "Generalized design of high performance shunt active power filter with output LCL filter," *IEEE Trans. Ind. Electron.*, vol. 59, no. 3, pp. 1443–1452, Mar. 2012

[10] J. Kukkola and M. Hinkkanen, "Observer-based state-space current control for a three-phase grid-connected converter equipped with an LCL filter," *IEEE Trans. Ind. Appl.*, vol. 50, no. 4, pp. 2700–2709, Jul./Aug. 2014

[11] C. A. Busada, S. Gomez Jorge, and J. A. Solsona, "Full-state feedback equivalent controller for active damping in LCL-filtered grid-connected inverters using a reduced number of sensors," *IEEE Trans. Ind. Electron.*, vol. 62, no. 10, pp. 5993–6002, Oct. 2015

[12] J. Dannehl, M. Liserre, and F. W. Fuchs, "Filter-based active damping of voltage source converters with LCL filter," *IEEE Trans. Ind. Electron.*, vol. 58, no. 8, pp. 3623–3633, Aug. 2011

[13] J. Xu, S. Xie, and T. Tang, "Active damping-based control for grid-connected LCL -filtered inverter with injected grid current feedback only," *IEEE Trans. Ind. Electron.*, vol. 61, no. 9, pp. 4746–4758, Sep. 2014

[14] X. Wang, F. Blaabjerg, and P. C. Loh, "Grid-current-feedback active damping for LCL resonance in grid-connected voltage-source converters," *IEEE Trans. Power Electron.*, vol. 31, no. 1, pp. 213–223, Jan. 2016

[15] E. Rodriguez-Diaz, F. D. Freijedo, J. C. Vasquez, and J. M. Guerrero, "Analysis and comparison of notch filter and capacitor voltage feedforward active damping techniques for LCL grid-connected converters," *IEEE Trans. Power Electron.*, vol. 34, no. 4, pp. 3958–3972, Apr. 2019

[16] V. Miskovic, V. Blasko, T. Jahns, A. Smith, and C. Romenesko, "Observer based active damping of LCL resonance in grid connected voltage source converters," *IEEE Trans. Ind. Appl.*, vol. 50, no. 6, pp. 3977–3985, Nov./Dec. 2014.

[17] M. Hanif, V. Khadkikar, W. Xiao, and J. L. Kirtley, "Two degrees of freedom active damping technique for LCL filter based grid connected PV systems," *IEEE Trans. Ind. Electron.*, vol. 61, no. 6, pp. 2795–2803, Jun. 2014.

[18] J. Dannehl, C. Wessels, and F. W. Fuchs, "Limitations of voltage-oriented PI current control of grid-connected PWM rectifiers with LCL filters," *IEEE Trans. Ind. Electron.*, vol. 56, no. 2, pp. 380–388, Feb. 2009

[19] J. Wang, J. D. Yan, L. Jiang and J. Zou, "Delay-dependent stability of single-loop controlled grid-connected inverters with LCL filters," *IEEE Trans. Power Electron.*, vol. 31, no. 1, pp. 743–757, Jan. 2016

[20] D. Pan, X. Ruan, C. Bao, W. Li, and X. Wang, "Capacitor-current-feedback active damping with reduced computation delay for improving robustness of LCL-type grid-connected inverter," *IEEE Trans. Power Electron.*, vol. 29, no. 7, pp. 3414–3427, Jul. 2014.

[21] J. Yin, S. Duan, and B. Liu, "Stability analysis of grid-connected inverter with LCL filter adopting a digital single-loop controller with inherent damping characteristic," *IEEE Trans. Ind. Informat.*, vol. 9, no. 2, pp. 1104–1112, May 2013.

[22] S.G. Parker, B. P. McGrath, and D. G. Holmes, "Regions of active damping control for LCL filters," *IEEE Trans. Ind. Appl.*, vol. 50, no. 1, pp. 424–432, Jan./Feb. 2014.

[23] X. Li, X. Wu, Y. Geng, X. Yuan, C. Xia, and X. Zhang, "Wide damping region for LCL-type grid-connected inverter with an improved capacitor-current-feedback method," *IEEE Trans. Power Electron.*, vol. 30, no. 9, pp. 5247–5259, Sep. 2015

[24] M. Ben Saïd-Romdhane, M. W. Naouar, I. Slama-Belkhodja, and E. Monmasson, "Robust active damping methods for LCL filter-based grid-connected converters," *IEEE Trans. Power Electron.*, vol. 32, no. 9, pp. 6739–6750, Sept. 2017

[25] C. Liu, X. Zhang, L. H. Tan and F. Liu, "A novel control strategy of LCL-VSC based on notch concept," in *Proc. IEEE Int. Symp. PEDG Syst.*, Hefei, China, 2010, pp. 343–346

[26] J. Ma, X. Wang, F. Blaabjerg, L. Harnefors, and W. Song, "Accuracy analysis of the zero-order hold model for digital pulse width modulation," *IEEE Trans. Power Electron.*, vol. 33, no. 12, pp. 10826–10834, Dec. 2018.

[27] X. Wang, L. Harnefors and F. Blaabjerg, "Unified impedance model of grid-connected voltage-source converters," *IEEE Trans. Power Electron.*, vol. 33, no. 2, pp. 1775–1787, Feb. 2018